Improved Ion Extraction from a Linear Octopole Ion Trap: SIMION Analysis and Experimental Demonstration

Bruce E. Wilcox, Christopher L. Hendrickson, and Alan G. Marshall*

Ion Cyclotron Resonance Program, National High Magnetic Field Laboratory, Department of Chemistry, Florida State University, Tallahassee, Florida, USA

Externally generated ions are accumulated in a linear octopole ion trap before injection into our 9.4 T Fourier transform ion cyclotron resonance (FT-ICR) mass analyzer. Such instrumental configuration has previously been shown to provide improved sensitivity, scan rate, and duty cycle relative to accumulated trapping in the ICR cell. However, inefficient ion ejection from the octopole currently limits both detection limit and scan rate. SIMION 7.0 analysis predicts that a dc axial electric field inside the linear octopole ion trap expedites and synchronizes the efficient extraction of the octopole-accumulated ions. Further SIMION analysis optimizes the ion ejection properties of each of three electrode configurations designed to produce a near-linear axial potential gradient. More efficient extraction and transfer of accumulated ions spanning a wide *m/z* range promises to reduce detection limit and increase front-end sampling rate (e.g., to increase front-end resolution for separation techniques coupled with FT-ICR mass analysis). Addition of the axial field improves experimental signal-to-noise ratio by more than an order of magnitude. (J Am Soc Mass Spectrom 2002, 13, 1304–1312) © 2002 American Society for Mass Spectrometry

The interface of electrospray ionization (ESI) with Paul [1, 2] and Penning [3, 4] traps is a popular and powerful technique for mass analysis of polar analytes of limited or zero volatility (e.g., peptides, proteins, nucleotides, phospholipids, oligosaccharides, environmental mixtures, etc.). However, electrospray is a temporally continuous ion source, whereas mass analysis in an ion trap (Paul or Penning) is an inherently pulsed process, thereby limiting the experimental sensitivity and duty cycle. A general method for increasing the sample utilization and sensitivity of ESI-generated ions in Paul or Penning traps is to accumulate electrosprayed ions externally in a linear multipole ion trap during mass analysis, and then eject those ions for mass analysis during the next accumulation cycle [5–11]. Collisional damping within the external trap also cools and focuses the ions for improved transmission to the final ion trap analyzer. Ion external accumulation and storage improves signal-to-noise ratio and mass resolving power, and increases the duty cycle to nearly 100% [6].

The aspect (length-to-width) ratio of an external end-capped multipole ion trap is chosen to be much larger than unity, so as to trap a large number of ions without excessive space-charge repulsion. However, because the end cap dc potential field in such a trap does not penetrate very far into the central region of the multipole, ions are not all ejected simultaneously on application of a dc potential difference between the two end caps. Ions of different axial position and/or velocity inside the trap will be ejected at different times, thereby reducing the efficiency of subsequent gated trapping as those ions enter the final analyzer trap. The rate of ion ejection also depends on space charge [11] and thus depends on the total number of ions as well.

It is therefore desirable to introduce an axial electric potential gradient (i.e., an axial electric field) to increase the efficiency of ion ejection from an external multipole ion trap. For example, generation of an axial electric field by segmenting the multipole rods themselves has been extensively characterized [11–17]. Other methods for producing an axial electric field include conical (rather than fixed-diameter) multipole rods [18], offsetting one end of the multipole from the central (z-) axis [14], encasing the multipole with segmented rings [15, 19], and the insertion of electrodes between parallel rods [20, 21].

Here, we seek to optimize ion ejection from a multipole device by introducing an axial electric field inside the multipole, in a new (mechanically and electronically simple) way, without distorting the multipole potential field needed to confine, accumulate, store, cool, and focus the ions. We present extensive SIMION 7.0 modeling to show that application of a modest (e.g., 10 V) dc

Published online September 25, 2002

Address reprint requests to Dr. A. G. Marshall, National High Magnetic Field Laboratory, Florida State University, 1800 East Dirac Drive, Tallahassee, FL 32310, USA. E-mail: marshall@magnet.fsu.edu

*Also at the Department of Chemistry and Biochemistry, Florida State University, Tallahassee, FL 32310, USA.

1044-0305/02/$20.00
PII S1044-0305(02)00622-0

Received July 19, 2002
Accepted August 6, 2002

potential to angled wires placed between adjacent parallel octopole rods achieves just such a goal. The simulations predict that ions of $500 < m/z < 2000$ and arbitrary initial axial position within the trap can be ejected nearly simultaneously (e.g., during an interval of ~250 μs), compared to a spread of several ms without the axial potential gradient.

Theory

A short review of the quadrupole mass filter helps to explain the operation of an octopole for ion transfer and storage. A perfect quadrupole mass filter consists of four infinitely extended parallel rod electrodes, each of hyperbolic cross-section, whose centers are equally spaced around the axis of a right circular cylinder [22]. Application of equal voltages of opposite sign to adjacent rods produces a potential that varies as $(x^2 - y^2)$. The mass filter is activated by applying an rf potential, $V \cos(\omega t)$ to one pair of opposed electrodes and a 180° phase-shifted potential $(-V \cos(\omega t))$ to the other pair. Similarly, a positive dc potential is applied to one pair of opposed rods and a corresponding negative potential of the same magnitude is applied to the other pair. It is possible to solve the ion motion in the x and y directions independently because they are uniquely decoupled in the quadrupole. There is no axial force acting on an ion on the z-axis of the quadrupole mass filter; thus, it is necessary to apply an additional dc potential gradient (i.e., dc electric field) along the z-direction in order to push ions in the z-direction (see below).

The quadrupole mass filter operates on the principle that ions of only certain m/z ratios will maintain a stable trajectory within the electrode configuration for particular rf and dc potentials [22, 23]. The ion equation of motion reduces to a Mathieu equation [22], characterized by the so-called "stability" parameters

$$a_u = \frac{8zeU}{m\omega^2 r_0^2} \text{ (S.I. units)} \quad (1)$$

and

$$q_u = \frac{4zeV}{m\omega^2 r_0^2} \text{ (S.I. units)} \quad (2)$$

in which U is the applied dc potential, V is the zero-to-peak amplitude of the applied rf potential, z is the number of elementary charges per ion, e is the elementary charge, m is ion mass, $\omega = 2\pi\nu$ is the rf angular frequency rad s^{-1}) and ν is the rf frequency (Hz), and r_0 is one half of the closest distance between opposed rods. The subscript, u, represents x or y. In a graph whose axes are a_u and q_u, a "stability diagram" defines a unique boundary within which ions of those a_u and q_u values execute stable trajectories inside the quadrupole. In the presence of a collision ("buffer") gas, the quadrupolar field radially focuses ions towards the central axis of the quadrupole. At high m/z, ion radial motion is dominated by the dc potential, whereas the radial motion of ions of low m/z is controlled mainly by the rf potential (because ions of low m/z can respond more rapidly to a changing rf field). At zero-magnitude dc voltage and a given rf voltage magnitude, ions below a cutoff m/z value are unstable and will not pass through the (high-pass) quadrupole mass filter. As the rf potential magnitude increases, ions of progressively higher m/z become unstable. Increasing both the a_u and q_u values in fixed ratio defines a "scan line" that intersects the stability diagram, thereby narrowing the range of m/z values for which ion motion is stable. Unit mass resolution is obtainable up to m/z ~4000 in that mode of operation. Conversely, operating a quadrupole mass filter in the rf-only mode results in passing ions of the widest possible m/z range through the filter.

The octopole operates under the same principles as the quadrupole, but with some important differences. First, the x-y force acting on an ion is no longer linear, because the potential varies as $(x^4 - 6x^2y^2 + y^4)$. Thus, ion x- and y-motions are coupled. Second, in a multipole of order, $2n$ (i.e., $n = 2$ for a quadrupole, $n = 3$ for a hexapole, $n = 4$ for an octopole), the effective restoring force varies as r^{n-1} (e.g., r for a quadrupole versus r^3 for an octopole). Thus, ions can extend farther radially in an octopole than in a quadrupole. Third, the natural ("secular") frequencies of ion oscillation in a quadrupole are independent of ion location inside the region bounded by the rods, whereas ion natural motional frequencies in an octopole depend on ion position and velocity within the device. Fourth, the "stability" diagram for an ion in an octopole also depends on ion position and velocity. Extensive theoretical analysis [19, 24] concludes that the octopole is well suited for ion transport and storage but not high-resolution mass analysis.

Other significant differences between a quadrupole and an octopole (or other higher order multipoles) are the charge capacity and stability of ions within the device. Recent literature [16] indicates that an octopole has twice the charge capacity of a quadrupole for low-energy ions and is stated to be three times better for ions near their CID dissociation threshold. However, the charge density of the ion cloud in a quadrupole is relatively uniform radially whereas the octopole charge density increases with increasing radial displacement. Subsequently, the ion ejection properties of a quadrupole are proposed [16] to have potentially higher efficiency due to the higher charge density on-axis. Conversely, the range of stable m/z values of an octopole is wider than that for a quadrupole [25].

Simon Modeling

Ion trajectory modeling was performed with SIMION 7.0 software (SIMION 7.0 beta, D. A. Dahl, Idaho National Engineering Laboratory, Idaho Falls, ID). Initial modeling experiments were based on the linear ion

trap (LIT) in our previously described 9.4T FT-ICR MS instrument [5, 6]. Due to memory constraints, the potential array size was based on an octopole 7.5 cm in length (rather than 15 cm as in our instrument). The three-dimensional rectilinear potential array was 3,840,000 voxels (i.e., volume elements) with a grid unit spacing of 0.0635 mm. The resulting potential differs from a true octopolar potential only at locations very close to each rod. The octopole potential array file specifies a radial distance, $r_0 = 0.238$ cm, from the z-axis to the nearest surface of each (circular cross-section) octopole rod and a rod radius, $r_{rod} = 0.079$ cm. The ratio, $r_{rod}/r_0 = 0.332$ was chosen to match that in our instrument [6, 26], and it closely approximates the ratio (0.355) claimed to produce an optimized octopolar potential for rods of circular cross section [27]. In any case, it is not clear that a pure octopolar potential is required for efficient ion storage and transfer. The placement of an end cap (a circular 1.59 cm diameter disk, 0.0635 cm thick, with a 0.238 cm diameter circular hole centered on the z-axis) at each end of the octopole serves to confine ions axially by creating an axial potential well when an appropriate dc potential (typically 10 V) is applied to each end cap. Modeling of the cusped-ring design was performed by use of 13 cusped-ring electrodes encasing the octopole rods between the endcaps. Each electrode has an outer radius of 0.9525 cm, and length 0.495 cm, with a 0.0762 cm spacing between adjacent electrodes. The cusped-ring electrodes have an inner radius of 0.432 cm and a 0.0508 cm spacing between the cusped-ring electrode inner surface and the outer surface of each octopole rod. Thirteen equal-length sections were also used to model the segmented octopole. The axial fields of the rings and segments were determined by recording a single ion trajectory and subsequent axial kinetic energy (initially room temperature) from octopole entrance to exit. An rf potential was not present during that experiment. Due to memory constraints (the tilted wires are too small to be accurately modeled), the wire octopole was modeled by a series of 2-D arrays with an incrementally larger radial wire position. The dc-axial potential was determined for each of these arrays. These values were then plotted and fitted to a single exponential decay. That dc-axial field was then analytically expressed within a SIMION user program to perform the 3-D simulations. It should be noted that the methods described here to calculate the imposed axial field of the rings, segments, and wires do not account for the axial pseudopotential present at the ends of the octopole (Figures 2 and 6). However, the axial pseudopotential is explicitly included in the ion extraction simulations and experimental data (Figures 7–9). An rf voltage of amplitude, 1000 $V_{p\text{-}p}$, and frequency, $\Omega/2\pi = 1.2$ MHz was applied with 180° phase difference between adjacent octopole rods. The SIMION potential array was updated at intervals of 0.0083 μs. All SIMION simulations were performed on a custom-built PC-compatible computer comprised of dual Intel 1 GHz P-III processors and 1 GB of memory.

A SIMION 7.0 user program simulated all applied electrode voltages and necessary timing intervals for ion trapping and ejection. A user-defined time delay was added to the program to control the time period necessary for ions to reach equilibrium inside the LIT after their generation. Ion initial positions were generated randomly along the z-axis within the octopole for all trapping and ejection simulations by use of the random ion generator in the SIMION Ion Trap demo. Ions are positive and have mass-to-charge ratio, $m/z = 1000$, unless otherwise stated. Ions are considered to be ejected from the octopole if they pass through the exit end cap and leave the potential array; at that instant, the ion kinetic energy, x position, and time elapsed since application of the dc voltage are recorded. All ions begin with room temperature kinetic energy (0.03855 eV), with no collisional cooling [28]. Ion–ion Coulomb repulsion was not taken into consideration in these simulations. All SIMION simulations were performed at a calculation level of +3.

Results and Discussion

We now compare SIMION ion trajectories for three linear ion trap configurations (see Figure 1) designed to generate an axial electric field to synchronize and expedite ion ejection. For reference, a linear trap without an axial field was approximated by grounding the wires in the octopole wire design of Figure 1 (bottom).

Potential Energy Profile Inside a Linear Octopole Ion Trap

In the absence of modifications, the axial dc electric potential in an octopole is essentially flat from the entrance to the exit of the multipole, except for a steep gradient near each end (Figure 2, top). An axial electric field can be created inside a multipole by segmenting each of the multipole rods into several short sections (Figure 1, top) and applying monotonically (e.g., linearly) varied dc potentials to successive segments to create an axial gradient [11, 13–15]. The spacing between each segment was optimized to minimize field distortion and still satisfy practical limitations of construction. The potential gradient along the central z-axis of a segmented octopole (shown in Figure 2) is linear, but the discontinuities between successive segments lead to ripples in the gradient that could complicate future attempts to achieve spatial focusing at the ICR cell. In any case, mounting, aligning, and electrically connecting the large number of segments is mechanically complex and difficult. We are thus led to consider other ways to achieve a smooth electric field gradient in a mechanically simpler way.

Another approach is to encase the multipole inside a conductive cylinder segmented into equally spaced rings, and apply monotonically (e.g., linearly) varied dc voltage to successive rings [13, 19]. The axial potential

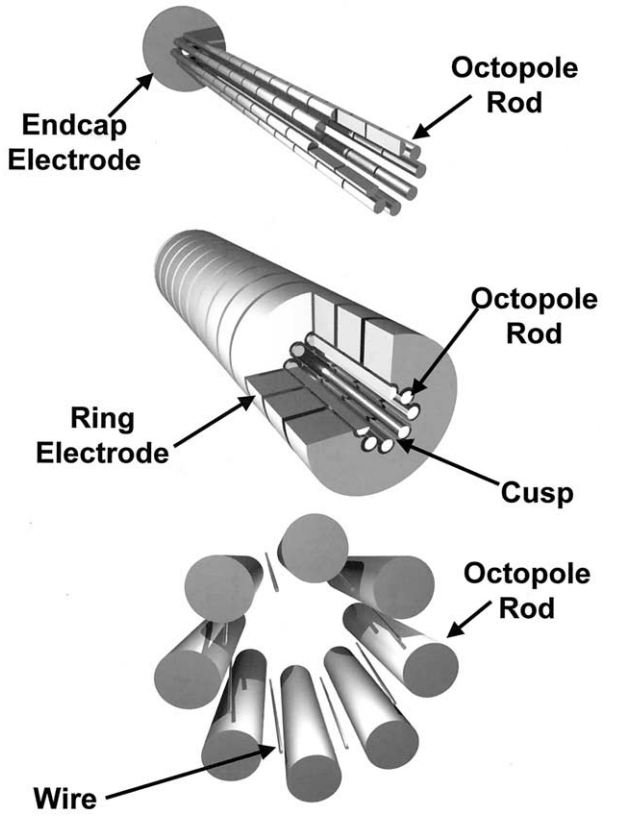

Figure 1. Three electrode configurations, each designed to produce an axial electric potential gradient inside an octopole ion trap. Top: Axially segmented octopole rods. Middle: Unbroken octopole rods enveloped by a series of cusped rings [15, 19]. Bottom: A new design in which angled (100 μm diameter) wires are placed between adjacent (unbroken) rods, for improved axial electric field penetration.

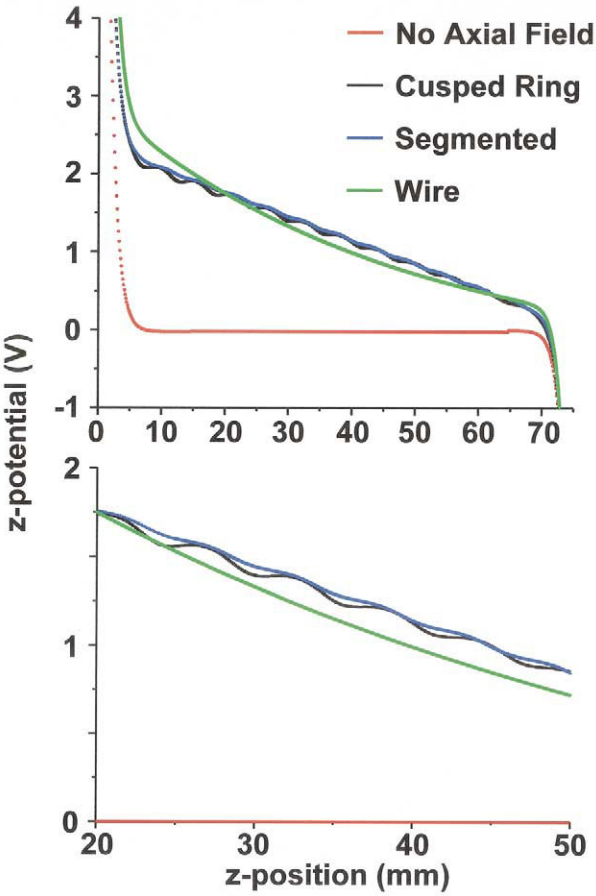

Figure 2. SIMION 7.0 representation of the z-axis electric dc potential contour inside an octopole, for each of the configurations of Figure 1. Top: An unsegmented octopole produces a significant z-axis potential gradient only in regions very close to either end cap. Each of the three configurations of Figure 1 produces an electric potential gradient that is approximately linear throughout the region between the octopole end caps. Bottom: Scale expansion of the same plot for the region spanning the midpoint between the two end caps reveals that the segmented octopole (Figure 1, top) and cusped-ring (Figure 1, middle) configurations generate "ripples" in the potential gradient, arising from the discontinuities between the rod or ring segments. The angled-wire configuration (Figure 1, bottom) yields a smoother but less linear (actually exponential) potential gradient. All SIMION potentials include the contribution from the end caps.

(not shown) of such an arrangement resembles that of the segmented multipole (i.e., ripples again arise from the discontinuities between adjoining rings). Moreover, relatively high voltages must be applied to ensure sufficient field penetration between the multipole rods to act on ions within the multipole (e.g., ~500 V). We therefore proposed a new design, in which the rings are brought closer to the multipole axis by embedding the multipole rods in cusp-shaped recesses in the enveloping rings (Figure 1, middle). An axial potential gradient may be generated by applying a single dc potential, divided by a resistor between each adjacent pair of rings.

Simulations establish that the cusped-ring electrode configuration provides a significantly improved field penetration (1.25 versus 0.25% of the applied potential) compared to rings placed just outside the multipole. Figure 2 shows the potential energy profile along the multipole central z-axis for the cusped-ring octopole (Figure 1b) with 5 mm long electrodes and a spacing of 0.76 mm between the cusped rings. It is clear that the ripples in the otherwise linear potential gradient are much more pronounced than for segmentation of the multipole rods. Additionally, these ripples appear as small potential wells in the axial field between each cusped-ring electrode near the multipole entrance (Figure 2), resulting from the electrode placement. Squeezing the rings closer together reduces the ripples, but also makes mechanical alignment more difficult. A small percentage of ions positioned between cusped-ring electrodes on application of the dc potential will remain trapped in these small ripples longer than the LIT extraction event, thus decreasing ion transfer efficiency. However, these ripples (acting as potential wells) are deep enough only between the first few cusped-ring electrodes to store room temperature ions.

The ripples in the axial dc potential gradient generated by axially segmented multipole rods or an enveloping segmented cylinder (Figure 1, top and middle)

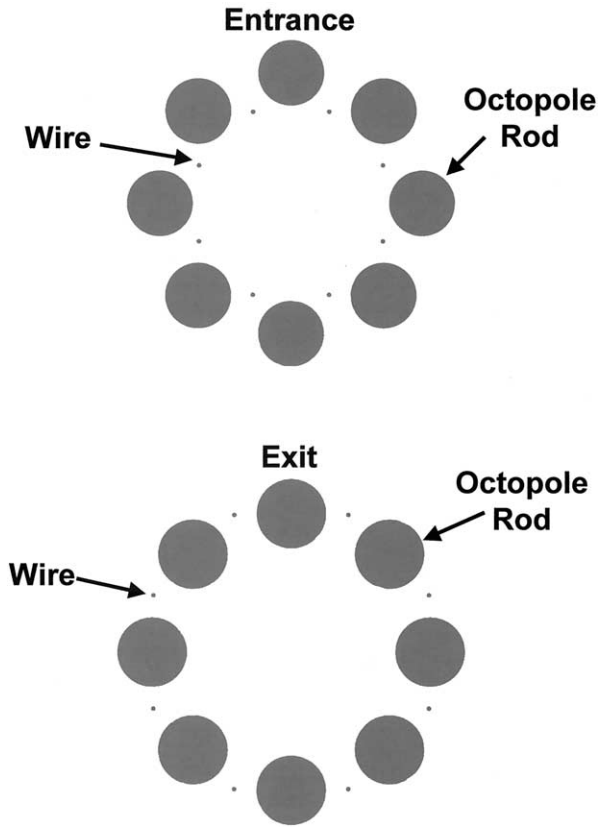

Figure 3. Transverse sections of the electrode configuration of Figure 1, bottom, in which angled wires are centered between adjacent octopole rods so as to generate an axial electric potential field. Top: At the entrance to the octopole, the radial displacement of each wire is r_0, for maximum field penetration. Bottom: At the exit from the octopole, the wire radial position has increased to (r_0 + 1000 μm) from the z-axis.

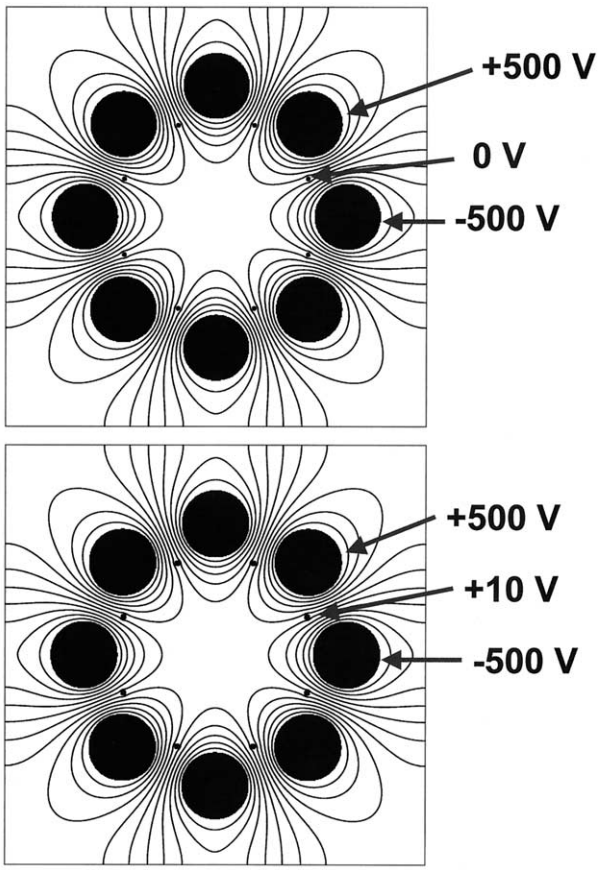

Figure 4. Transverse sections, showing electric field (rf + dc) isopotentials for the octopole with angled wires at the rf maximum potential. No significant difference in the radial potential is observable between the storage 0 V dc (top diagram) and ejection +10 V dc (bottom diagram) mode of operation.

result in a spatially nonuniform force on ions inside the multipole. As we shall later show, such a force results in a wider spread in exit (ejection) times for ions at different initial axial positions within the multipole. One might therefore hope that an axial dc potential that varies smoothly from one end of the multipole to the other might result in better synchronization of the exiting ions. To that end, we next consider a new electrode configuration in which a wire is centered between every two adjacent rods of a linear multipole (Figure 1, bottom). A single dc potential is applied to all wires, and the axial dc potential gradient is achieved by angling the wires so that the wires are closer to the z-axis at the multipole entrance (Figure 3, top) than at the multipole exit (Figure 3, bottom). Figure 2 shows the resulting ripple-free axial dc electric potential gradient.

The extent to which the angled wires of Figure 1 (bottom) distort the multipole electric field may be evaluated from the electric isopotentials at an instant of maximum rf potential (Figure 4) and an instant of rf zero crossing (Figure 5). Even at the entrance to the multipole, where the wires penetrate closest to the multipole central z-axis, the dc potential from the wires produces no obvious change in the overall radial electric isopotentials at an instant of rf maximum (Figure 4), a result expected because of the placement of the wires halfway between each pair of rods (i.e., approximately along a node of the potential distribution). At an rf potential zero crossing (Figure 5), the applied dc wire potential clearly adds a small (note the values of the isopotential contours) dc 16-pole (hexadecapole) component to the octopolar field. The small 16-pole contribution is unlikely to affect ion transmission through the multipole, and we observed no effect in our simulations.

The strength and shape of the continuous axial electric field generated by the introduction of angled wires depends on the wire diameter and position. For a given applied dc voltage, a larger wire diameter produces a greater dc axial electric field magnitude, particularly at the entrance to the multipole. The dc axial field near the octopole exit is nearly independent of wire diameter. Thus, a larger wire diameter increases not only the axial potential magnitude, but also the gradient of the axial potential and thus the axial electric field magnitude. Larger wire diameter also increases the magnitude of the 16-pole contribution due to greater dc field penetration. Finally, Figure 2 and Figure 6 show

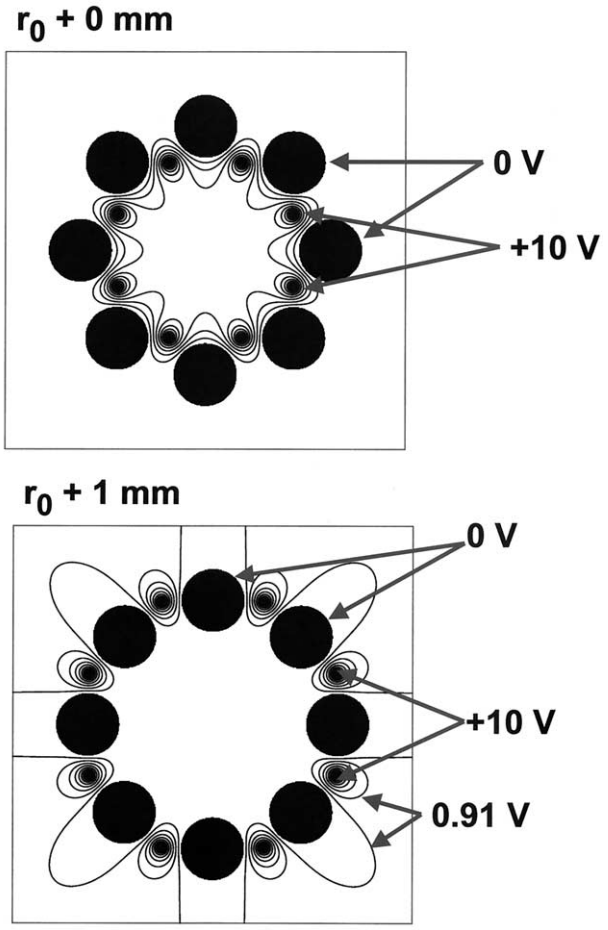

Figure 5. Transverse sections, as in Figure 4, but plotted as the rf potential crosses zero. The isopotentials change noticeably only in the ejection mode (+10 V) of operation. The largest changes occur at the octopole entrance (r_0), where the wires add a 16-pole component to the octopolar field from the rods. The additional contribution becomes negligible near the octopole exit (r_0 + 1000 μm).

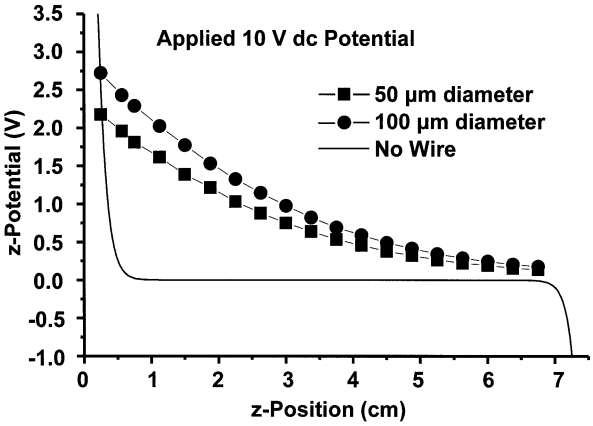

Figure 6. SIMION 7.0-generated z-axis electric potential (V) for two finite-diameter (50 and 100 μm) wires placed at the same angle with respect to the octopole z-axis (r_0 at the octopole entrance and r_0 + 1 mm at the exit) and compared to the absence of wires. A constant dc potential of 10 V is applied to each wire. The axial field is determined by the radial displacement of the wire from the z-axis of the octopole. The larger-diameter wire produces a larger axial potential at the entrance to the octopole, and the axial potential becomes essentially independent of wire diameter at the exit from the octopole. The SIMION potentials in this Figure do *not* include contributions from the end caps, so as to emphasize just the contributions from the angled wires.

that ions initially closer to the LIT entrance have farther to travel, but undergo more initial acceleration than ions close to the LIT exit. Thus, at some axial distance from the multipole exit, there will be some spatial focusing of the ions initially in the multipole—ideally, inside the ultimate ion trap mass analyzer. Moreover, altering the applied voltage and/or axial field will change the location at which ions become focused. The ultimate ability of the device to focus ions at the ICR cell will be described separately.

Ion Extraction from an Octopole Ion Trap

Ion extraction from an octopole with and without an axial field was characterized by SIMION 7.0 ion trajectory simulations. An axial dc electric potential gradient of ~0.3 V/cm was generated by the segmented multipole, cusped-rings, and angled-wire configurations of Figure 1 only during the ion ejection event. A gradient of 0.3 V/cm was previously shown to optimize the interface of a segmented quadrupole with an FT-ICR mass analyzer [11].

Figure 7 shows time profiles for ejection of 2300 ions of *m/z* 1000, located at random initial axial positions within a 7.5 cm-long octopole and average electric field of 0.3 V/cm for each of the three configurations of Figure 1. In the absence of an axial electric field, the distribution of ion exits from the octopole spread out

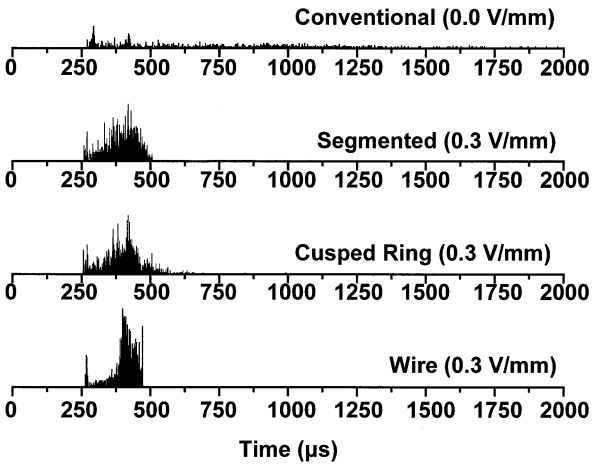

Figure 7. Relative number of ejected ions versus time elapsed following application of a dc potential for 2300 ions (*m/z* 1000) initially confined in each of the octopole configurations of Figure 1. If no axial field is present, ions are ejected over a period of several ms (top diagram). Application of an average 0.3 V/cm axial field in any of the three configurations significantly compresses the time span for ion ejection. Note that the angled-wire design provides the greatest ejection time compression, which should lead to highest subsequent capture efficiency in the trapped-ion cell.

over an interval of several milliseconds. Thus, Figure 7 demonstrates that all three configurations improve by an order of magnitude the speed and simultaneity of ion ejection compared to a linear octopole without an axial field. Ion ejection efficiency approaches 100% for the segmented-multipole and angled-wire designs and ~95% for the cusped-ring configuration.

Increasing the axial dc electric field to 2.0 V/cm results in steadily decreasing ion ejection efficiency for the segmented and cusped-ring designs, whereas the wire design maintains ~100% ion ejection efficiency. Figure 7 shows that ions exit the octopole over a time span of ~400, 250, and 200 μs for the cusped-ring, segmented-octopole, and angled-wire configurations, respectively. The wire design gives the shortest ion ejection period (200 μs). The narrower ejection profile for the angled-wire design increases the probability of subsequent capture of all stored ions in a Paul or Penning trap. A temporally short ion packet ejected from a linear multipole ion trap could improve the performance characteristics of other mass analyzers as well (e.g., TOF). The sharp onset in ion ejection for each design derives from ions initially closest to the octopole exit end cap, which is switched to a −10 V dc potential simultaneously with the axial potential gradient creation.

As noted above, ions closer to the multipole entrance undergo stronger and longer acceleration than ions nearer to the multipole exit, and the effect will depend on *m/z*. Figure 8 shows SIMION 7.0-calculated ion exit time distributions for ions spanning a mass-to-charge ratio range typical of electrospray ionization: m/z = 500, 1000, and 2000. Although ions of different *m/z* are not ejected simultaneously, the distribution of exit times still spans a sufficiently narrow range relative to the typical length of time available for capture of ions in a Penning trap by gated trapping [29]. We established that the curious "structure" of the ion ejection profiles results from initial ion conditions within the simulation (i.e., the initial conditions were not truly random), but those parameters do not alter the overall observed trend.

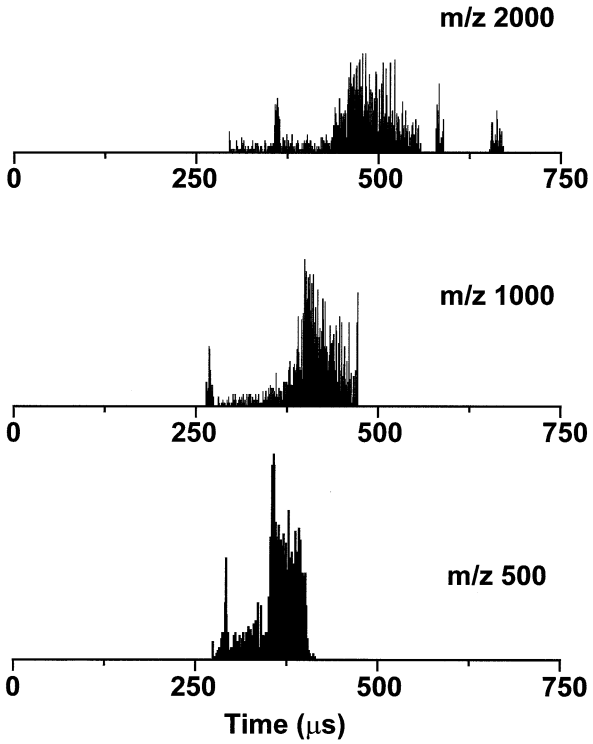

Figure 8. Ejection profiles as in Figure 7, but this time for 2300 ions of *m/z* 2000 (top), 1000 (middle), and 500 (bottom) exiting the octopole storage device of Figure 1 (bottom). An axial electric field is created by application of a +10 V dc potential to the wires between the rods. Although there is some *m/z* discrimination, most of the ions (irrespective of mass) are ejected in less than 500 μs.

Preliminary Experimental Results

Based on the these simulations, we constructed an angled-wire octopole ion trap for our homebuilt 7 T FT-ICR mass spectrometer [30–33]. Figure 9 shows the significant improvement in signal-to-noise (S/N) ratio for 100 femtomole/μL electrosprayed bovine ubiquitin accumulated for 2 s. The improvement is due solely to more effective ejection of ions stored within the linear octopole ion trap, because of the added axial field. The S/N ratio improvement is maintained across the full charge-state distribution of bovine ubiquitin. These initial experimental results validate the accuracy of the computer simulation predictions from SIMION 7.0. It is interesting to note that the wire potential required for optimal ejection was 40 V, compared to 10 V in the simulations. One explanation is that the space charge of the experimental ion cloud was sufficient to form a nonneutral plasma, which can shield the bulk of the cloud from external fields [34, 35]. A higher voltage is

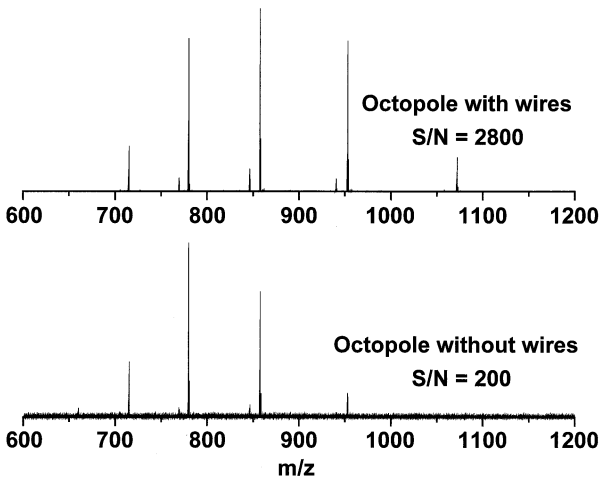

Figure 9. Mass-to-charge ratio spectra of electrosprayed bovine ubiquitin ions, ejected from an octopole with an axial field gradient created with wires (top) and without an axial field (bottom). Application of the axial field improves the signal-to-noise ratio by a factor of 14. A +40 V potential was applied to all wires simultaneously for the ejection of ions from the octopole toward the ICR cell.

then necessary for efficient extraction. Future work will test this hypothesis.

Conclusion

Here, we have simulated the trajectories of ions of several *m/z* ratios, following imposition of an axial dc potential gradient produced by each of three electrode configurations to an octopole ion trap (e.g., for ion accumulation external to a Paul or Penning trapped-ion mass analyzer). All three configurations shorten the ion exit time distribution by an order of magnitude, relative to an octopole trap without an axial dc potential gradient (i.e., with a dc potential difference applied between the two octopole end caps and rods. Of the three configurations, the angled-wire arrangement of Figure 1 (bottom) achieves ion ejection in the shortest time. Initial experiments confirm that extraction efficiency is improved such that signal-to-noise ratio improves by one order of magnitude. It is reasonable to project that a similar angled-wire approach should also apply to quadrupole and hexapole ion storage devices and to other external ion sources. The new angled-wire octopole external ion trap we have constructed, based on SIMION 7.0 simulation, will undergo extensive characterization in the near future. We are confident that it should significantly improve the detection limit and front-end sampling rate for FT-ICR mass analysis.

Acknowledgments

The authors thank John P. Quinn and Mark R. Emmett for technical assistance and Steven C. Beu for helpful discussion. This work was supported by the NSF National High-Field FT-ICR Mass Spectrometry Facility (CHE 99-09502), Florida State University, and the National High Magnetic Field Laboratory at Tallahassee, Florida.

References

1. McLuckey, S. A.; Van Berkel, G. J.; Goeringer, D. E.; Glish, G. L. Ion Trap Mass Spectrometry of Externally Generated Ions. *Anal. Chem.* **1994,** *66,* 689A–696A.
2. March, R. E. An Introduction to Quadrupole Ion Trap Mass Spectrometry. *J. Mass Spectrom.* **1997,** *32,* 351–369.
3. Marshall, A. G.; Hendrickson, C. L.; Jackson, G. S. Fourier Transform Ion Cyclotron Resonance Mass Spectrometry: A Primer. *Mass Spectrom. Rev.* **1998,** *17,* 1–35.
4. Hendrickson, C. L.; Emmett, M. R. Electrospray Ionization Fourier Transform Ion Cyclotron Resonance Mass Spectrometry. *Annu. Rev. Phys. Chem.* **1999,** *50,* 517–536.
5. Senko, M. W.; Hendrickson, C. L.; Pasa-Tolic, L.; Marto, J. A.; White, F. M.; Guan, S.; Marshall, A. G. Electrospray Ionization FT-ICR Mass Spectrometry at 9.4 tesla. *Rapid Commun. Mass Spectrom.* **1996,** *10,* 1824–1828.
6. Senko, M. W.; Hendrickson, C. L.; Emmett, M. R.; Shi, S. D.-H.; Marshall, A. G. External Accumulation of Ions for Enhanced Electrospray Ionization Fourier Transform Ion Cyclotron Resonance Mass Spectrometry. *J. Am. Soc. Mass Spectrom.* **1997,** *8,* 970–976.
7. Sannes-Lowery, K.; Griffey, R. H.; Kruppa, G. H.; Speir, J. P.; Hofstadler, S. A. Multipole Sotrage Assisted Dissociation, a Novel In-Source Dissociation Technique for Electrospray Ionization Generated Ions. *Rapid Commun. Mass Spectrom.* **1998,** *12,* 1957–1961.
8. Bier, M. E.; Park, M.; Syka, J. E. P. Ion Trap Mass Spectrometer System and Method. U.S.A. Patent 5,420,425, issued 30 May, 1995.
9. Rodgers, M. T.; Campbell, S.; Marzluff, E. M.; Beauchamp, J. L. Low-Energy Collision-Induced Dissociation of Deprotonated Dinucleotides: Determination of the Energetically Favored Dissociation Pathways and the Relative Acidities of the Nucleic Acid Bases. *Int. J. Mass Spectrom. Ion Processes* **1994,** *137,* 121–149.
10. Voyksner, R. D.; Lee, H. Investigating the Use of an Octopole Ion Guide for Ion Storage and High-Pass Mass Filtering to Improve the Quantitative Performance of Electrospray Ion Trap Mass Spectrometry. *Rapid Commun. Mass Spectrom.* **1999,** *13,* 1427–1437.
11. Belov, M. E.; Nikolaev, E. N.; Anderson, G. A.; Udseth, H. R.; Conrads, T. P.; Veenstra, T. D.; Masselon, C. D.; Gorshkov, M. V.; Smith, R. D. Design and Performance of an ESI Interface for Selective External Ion Accumulation Coupled to a Fourier Transform Ion Cyclotron Mass Spectrometer. *Anal. Chem.* **2001,** *73,* 253–261.
12. Javahery, G.; Thompson, B. A. A Segmented Radiofrequency-Only Quadrupole Collision Cell for Measurements of Ion Collision Cross Section on a Triple Quadrupole Mass Spectrometer. *J. Am. Soc. Mass Spectrom.* **1997,** *8,* 697–702.
13. Thomson, B. A.; Joliffe, C. L. Spectrometer with Axial Field. U.S.A. Patent 5,847,386, issued December 8, 1998.
14. Thomson, B. A.; Joliffe, C.; Javahery, R. RF-Only Quadrupoles with Axial Fields. *Proceedings of the 44th ASMS Conference on Mass Spectrometry and Allied Topics*; Portland, OR, May 1996; Vol. I, p 1155.
15. Thomson, B. A.; Jolliffe, C. L. Quadrupole with Axial DC Field. U.S.A. Patent 6,111,250, issued August 29, 2000.
16. Tolmachev, A. V.; Udseth, H. R.; Smith, R. D. Charge Capacity Limitations of Radio Frequency Ion Guides in their Use for Improved Ion Accumulation and Trapping in Mass Spectrometry. *Anal. Chem.* **2000,** *72,* 970–978.
17. Dodonov, A.; Kozlovsky, V.; Loboda, A.; Raznikov, V.; Sulimendov, I.; Tolmachev, A.; Kraft, A.; Wollnik, H. A New Technique for Decomposition of Selected Ions in Molecule Ion Reactor Coupled with Ortho-Time-of-Flight Mass Spectrometry. *Rapid Commun. Mass Spectrom.* **1997,** *11,* 1649–1656.
18. Mansoori, B. A.; Dyer, E. W.; Lock, C. M.; Bateman, K.; Boyd, R. K.; Thompson, B. A. Analytical Performance of a High-Pressure Radio Frequency-Only Quadrupole Collision Cell with an Axial Field Applied by Using Conical Rods. *J. Am. Soc. Mass Spectrom.* **1998,** *9,* 775–788.
19. Gerlich, D. Inhomogeneous RF Fields: A Versatile Tool for the Study of Processes with Slow Ions. *State-Selected and State-to-State Ion-Molecule Reaction Dynamics. Part 1. Experiment;* Ng, C.Y.; Baer, M., Eds; John Wiley and Sons Inc.: New York, 1992; *Vol. LXXXII,* pp 1–176.
20. Loboda, A.; Drutchnsky, A.; Loboda, O.; McNabb, J.; Spicer, V.; Ens, W.; Standing, K. Novel LINAC II Electrode Geometry to Create an Axial Field in a Multipole Ion Guide. *Proceedings of the 48th ASMS Conference on Mass Spectrometry and Allied Topics*; Long Beach, CA, June 2000; WPA016.
21. Loboda, A.; Krutchinsky, A.; Loboda, O.; McNabb, J.; Spicer, V.; Ens, W.; Standing, K. Novel Linac II Electrode Geometry for Creating an Axial Field in a Multipole Ion Guide. *Euro. J. Mass Spectrom.* **2000,** *6,* 531–536.
22. March, R. E.; Hughes, R. J. *Quadrupole Storage Mass Spectrometry.* Wiley: New York, 1989.
23. Dawson, P. H. *Quadrupole Mass Spectrometry and its Application.* Elsevier: Amsterdam, 1976.

24. Hagg, C.; Szabo, I. New Ion-Optical Devices Utilizing Oscillatory Electric Fields. III. Stability of Ion Motion in a Two-Dimensional Octopole Field. *Int. J. Mass Spectrom. Ion Processes* **1986,** *73,* 277–294.
25. Hagg, C.; Szabo, I. New Ion-Optical Devices Utilizing Oscillatory Electric Fields. IV. Computer Simulations of the Transport of an Ion Beam through an Ideal Quadrupole, Hexapole, and Octopole Operating in the RF-Only Mode. *Int. J. Mass Spectrom. Ion Processes* **1986,** *73,* 295–312.
26. Wang, Y.; Shi, S. D.-H.; Hendrickson, C. L.; Marshall, A. G. Mass-Selective Ion Accumulation and Fragmentation in a Linear Octopole Ion Trap External to a Fourier Transform Ion Cyclotron Resonance Mass Spectrometer. *Int. J. Mass Spectrom.* **2000,** *198,* 113–120.
27. Rama Rao, V. V. K.; Bhutani, A. Electric Hexapoles and Octopoles with Optimized Circular Section Rods. *Int. J. Mass Spectrom.* **2000,** *202,* 31–36.
28. Lock, C. M.; Dyer, E. W. Characterization of High Pressure Quadrupole Collision Cells Possessing Direct Current Axial Fields. *Rapid Commun. Mass Spectrom.* **1999,** *13,* 432–448.
29. Alford, J. M.; Williams, P. E.; Trevor, D. J.; Smalley, R. E. Metal Cluster ICR. Combining Supersonic Metal Cluster Beam Technology with FT-ICR. *Int. J. Mass Spectrom. Ion Processes* **1986,** *72,* 33–51.
30. Emmett, M. R.; White, F. M.; Hendrickson, C. L.; Shi, S. D.-H.; Marshall, A. G. Application of Micro-Electrospray Liquid Chromatography Techniques to FT-ICR MS to Enable High Sensitivity Biological Analysis. *J. Am. Soc. Mass Spectrom.* **1998,** *9,* 333–340.
31. Quenzer, T. L.; Emmett, M. R.; Hendrickson, C. L.; Kelly, P. H.; Marshall, A. G. High Sensitivity Fourier Transform Ion Cyclotron Resonance Mass Spectrometry for Biological Analysis with Nano-LC and Microelectrospray Ionization. *Anal. Chem.* **2001,** *73,* 1721–1725.
32. Senko, M. W.; Canterbury, J. D.; Guan, S.; Marshall, A. G. A High-Performance Modular Data System for FT-ICR Mass Spectrometry. *Rapid Commun. Mass Spectrom.* **1996,** *10,* 1839–1844.
33. Blakney, G. T.; van der Rest, G.; Johnson, J. R.; Freitas, M. A.; Drader, J. J.; Shi, S. D.-H.; Hendrickson, C. L.; Kelleher, N. L.; Marshall, A. G. Further Improvements to the MIDAS Data Station for FT-ICR Mass Spectrometry. *Proceedings of the 49th ASMS Conference on Mass Spectrometry and Allied Topics*; Chicago, IL, May 2001; WPM265.
34. Davidson, R. C. *Physics of Nonneutral Plasmas.* Addison-Wesley: Reading, MA, 1990.
35. Beu, S. C.; Hendrickson, C. L.; Vartanian, V. H.; Laude, D. A., Jr. Debye Shielding Mechanism for Trapping Ions Formed by Laser Desorption FT/ICR/MS. *Int. J. Mass Spectrom. Ion Processes* **1992,** *113,* 59–79.